International Journal of Control, Automation, and Systems 22(4) (2024) 1371-1384
http://dx.doi.org/10.1007/s12555-021-1105-x
ISSN:1598-6446 eISSN:2005-4092
http://www.springer.com/12555

Cascade Antidisturbance Control of Hydraulically Driven Bipedal Robots for High Dynamic Locomotion by Using Model Prediction and Task Hierarchical Optimization

Jie Huang, Huajie Hong, Nan Wang, Hongxu Ma, Honglei An, and Lin Lang*

Abstract: The development of hydraulically driven heavy legs that can withstand external interference for realizing the high-velocity dynamic walking of bipedal robots with eight degrees-of-freedom is challenging. Therefore, in this study, a cascade antidisturbance algorithm was proposed for highly dynamic trajectory tracking based on model prediction and task hierarchical optimization. First, in the upper layer, the time-sharing control framework of underactuated robots based on the single rigid body model ignoring the legs was designed. Linear model predictive control (MPC) was designed to calculate the contact force spin to control the posture and height of floating base in the stand phase. The desired foot location principle was used to control the forward and lateral velocity in the swing phase. Next, in the lower layer, task hierarchical optimization control (THOC) was designed to track the contact force spin predicted by MPC. The relaxation variable of the force spin was designed in the optimized variable and subsequently used to compensate for the contact force between single rigid body and whole-body dynamic models. Thus, the tie relationship was developed between the upper MPC and lower THOC. The control robustness of the proposed model under high-velocity locomotion and disturbance was verified by performing simulation experiments investigating high-velocity walking and external impact, and the fast walking velocity was increased from 2.15 m/s of nonlinear MPC to 2.5 m/s with accurate velocity tracking.

Keywords: Bipedal robot, cascade anti-disturbance control, high dynamic antidisturbance locomotion, model predictive control, task hierarchical optimization control.

1. INTRODUCTION

Bipedal robots can mimic the motion of humans and move freely in various complex environments. Anthropomorphic bipedal robots have been developed for use in entertainment, education, medical care, military, industrial manufacturing, harsh and dangerous environment operations, rescue, and other fields. Therefore, bipedal robots have attracted considerable research attention.

1.1. Related work

In 2001, Pratt *et al*. from Massachusetts Institute of Technology proposed the virtual model control (VMC) for the locomotion of a bipedal robot [1]. In 2003, Kajita *et al*. applied the decomposition momentum control, which is a whole-body control that considers the whole-body dynamics model, to the bipedal robot [2]. Subsequently, Sentis and Khatib developed a torque-based multi-level hierarchical control framework, namely the whole-body control (WBC) framework [3]. Because WBC was used extensively in the 2015 DRAPA Challenge Finals and achieved excellent performance, many teams have subsequently used WBC based on optimized solutions [4-6]. According to the task-level solution classification, WBC can be categorized into 1) WBC based on null-space projection [3,7,8]; 2) WBC based on weight stratification [9-11]; and 3) WBC based on sequence optimization [12]. A critical feature is that the whole-body model is considered in the controller design process; and has been widely applied on quadruped robots [13-15] and spider excavators [16]. Because the core is a single-step PD feedback control, this framework cannot satisfactorily resist disturbance and high velocity.

Studies on legged robots has focused on the model predictive control (MPC) framework, which has achieved excellent results in quadruped robots. In the framework, various models, such as inverted pendulum model [17,18], single rigid body model [19,20] and overall model [21,22],

Manuscript received December 28, 2021; revised November 1, 2022 and April 15, 2023; accepted May 22, 2023. Recommended by Senior Editor H. Jin Kim.

Jie Huang, Huajie Hong, Nan Wang, Hongxu Ma, and Honglei An are with the Intelligence Science College, National University of Defense Technology, No.109 Deya Road, Kaifu District, Changsha 410073, China (e-mails: {huangjiekaiming, opalqq}@163.com, acnwang@aliyun.com, {mhx1966, eric_nudt}@163.com). Lin Lang is with the Hunan University of Finance and Economics, No.139 Fenglin 2nd Road, Yuelu District, Changsha 410006, China (e-mail: langlin850214@sina.com).
* Corresponding author.

have been used in the application of legged robots. The model complexity directly affects the solution method and velocity, and the solution methods are developed into linear, nonlinear, robust [23-25] and learning MPC [26,27]. Because most of the current control objects are nonlinear time-varying systems, robust and learning MPCs can improve the robustness and tracking accuracy. However, the computational efficiency of the optimization algorithm limits the real-time application of these methods. Linear MPC (LMPC) using the simplified model provides inadequate dynamic characteristics.

In the bipedal robot considered in this study, the weight ratio of the legs to whole body is large because of the series leg mechanisms and electrohydraulic actuators. Therefore, the internal disturbance generated during fast walking can disturb robot balance. Furthermore, the external impact force acting on the floating base of the robot considerably affects locomotion stability. Therefore, this study focused on the control algorithm for resisting internal and external disturbances to achieve trajectory tracking and high-velocity locomotion.

1.2. Contributions

In this study, a cascade control framework, in which the leg dynamics are considered and linear model predictive control is combined with task hierarchical optimization control (THOC), was proposed to satisfy the antidisturbance control requirements of the bipedal robots for high-velocity locomotion and implement real-time control on the physical object. The details of the study are as follows:

a) In the upper layer, through the time-sharing control framework of under-actuated robot, a linear MPC controller based on a single rigid body model ignoring legs was designed to calculate the force spin, to control the posture and height of base link in the stand phase. At the same time, the foot location principle was used to control the forward and lateral velocity in the swing phase.

b) In the lower layer, the THOC was designed to track the force spin predicted by MPC. The relaxation variable of the force spin was designed in the optimized variable and used to compensate for contact force value between single rigid body model and complete dynamic model. Thus, the tie relationship was established between the upper MPC and the lower THOC.

MPC is used in the cascade control framework to improve the ability to resist disturbances. Furthermore, task sequence optimization control is used to integrate MPC during the stand period and desired foot location control during the swing period into one frame, to compensate for the dynamic disturbance from legs. Under task priority hierarchical optimization, accurately controlling the posture and height of floating base can better coordinate the robot balance, and the antidisturbance ability and locomotion velocity of the robot can be improved. Simulation experiments have verified the framework robustness under high-velocity locomotion and external impact. When the maximum velocity of the robot under nonlinear MPC (NMPC) reached 2.15 m/s, and the control framework increased the maximum walking velocity to 2.5 m/s.

The remainder of this paper is organized as follows: A bipedal robot system is introduced and the control problem is formulated in Section 2. The system model of robot is established in Section 3. The control framework was presented in Section 4. The cascade control using MPC and THOC are presented in Section 5. The validation of proposed model using simulation experiments is presented in Section 6. Finally, the conclusions and future work are summarized in Section 7.

2. PROBLEM FRAMEWORK

2.1. Introduction of bipedal robot

A hydraulically driven bipedal robot, developed by the legged robot laboratory, is used as a platform for conducting research (Fig. 1). The robot is approximately 0.4 m long and 0.45 m wide, with a maximum standing height of 0.9 meters and an overall weight of 45 kilograms, of which the weight of two legs is 14 kilograms. The three-dimensional (3D) locomotion of the robot is realized using only four active joints on a single leg. Electrohydraulic actuators are selected for joints because of their load-carrying ability.

A notable feature of this robot is the configuration of the linear contact strip feet without an active drive. This configuration has the following characteristics:

First, the configuration reduces the weight and inertia at the ends of legs. Because of the large volume and

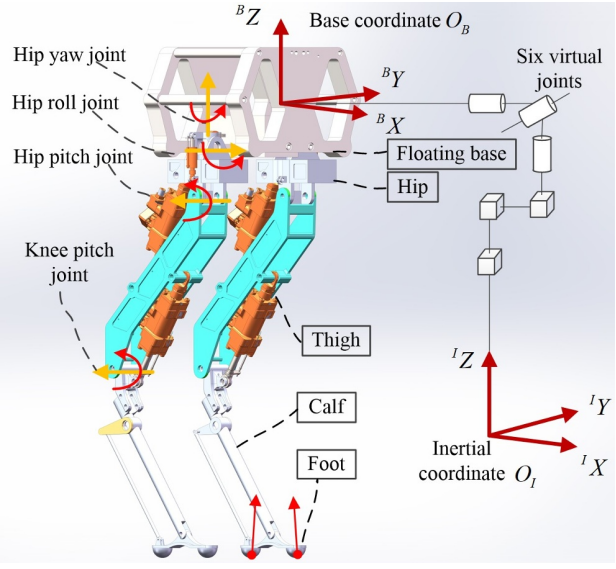

Fig. 1. The hydraulically driven bipedal robot.

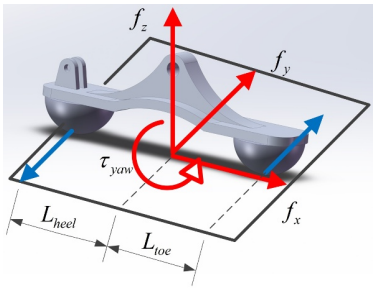

Fig. 2. The force and moment diagram.

weight of the electrohydraulic actuator, the use of the dual-degree-of-freedom active-driving flat foot configuration considerably increases the weight of the ankle mechanism. When the robot leg is in the rapid swing period, the high-inertia dynamics of ankle can severely hinder robot locomotion.

Second, the model satisfies the demand for yaw control. The most extreme method to reduce the ankle weight is the point foot form. Although this method is the best choice in planar bipedal robots, it exhibits several shortcomings in three-dimensional (3D) bipedal robots. When contacting the ground during walking, the single point foot is supported by the ground reaction force so that only linear forces are generated in the three directions of xyz, excluding the moments. Even if the robot has a yaw joint, a yaw moment is not observed on the ground. Therefore, effectively and stably realizing the yaw control of the robot is critical. Therefore, a strip foot outside the flat foot and point foot were considered. In the strip foot, the front and back two point feet are used to form a yaw moment rotating along the ground plane when the feet are in contact with the ground, and the robot realizes the yaw control during the stand phase. The force and moment diagram is shown in Fig. 2.

A small weight torque motor was used to drive the strip foot to achieve foot pitch control. The purpose of the study is to drive the strip foot to maintain a small angle and land smoothly during the swing phase and ensure the strip foot is in a passive state during the stand phase. The robot can pitch around the ankle joint and roll around the contact line, which is formed by the front and back points of striped foot with the ground and results in a motion similar to that of the point foot.

2.2. Problem

To satisfy large load capacity demands, direct-push electrohydraulic actuators are used in the robot. These actuators are directly connected to the corresponding joint. Therefore, the hip pitch joint and knee pitch joint actuators can only be installed at the corresponding joint of the leg.

First, the weight of actuator itself is large and typically concentrated on the legs. Moreover, the calf is typically made of steel to satisfy the strength requirements. Thus, the leg becomes heavy. According to the 3D design and physical weighing tests, the overall weight ratio of the legs to the robot is approximately 31%.

The internal high dynamic disturbance, which forms during fast walking, can disturb the balance of the robot. Furthermore, factors, such as external impacts acting on the robot base link and external disturbances, considerably affect the stable locomotion of the bipedal robot. Therefore, improving the antidisturbance control is a critical topic of research in the robotics field for the high-dynamic locomotion of the bipedal robots with large inertia legs.

3. SYSTEM MODEL

In order to analyze the antidisturbance motion control of the robot, the first task is to establish its motion system model, which consists of the kinematic model and the dynamic model.

3.1. Kinematic model

As shown in Fig. 1, inertial coordinate system $\boldsymbol{O}_I$ and base coordinate system $\boldsymbol{O}_B$ are established in the system. The robot pose $\mathbf{q}_b$ in the inertial coordinate system can be expressed as posture ${}^I\mathbf{q}_{b,r}$ and position ${}^I\mathbf{q}_{b,p}$ of the base coordinate system in the inertial coordinate system

$$\mathbf{q}_b = \left[{}^I\mathbf{q}_{b,r} \;\; {}^I\mathbf{q}_{b,p}\right]^T. \tag{1}$$

Combining n_b robot poses with n_a active drive joints, the generalized variable describing the motion of the bipedal robot is constructed as follows:

$$\mathbf{q} = \left[\mathbf{q}_b \;\; \mathbf{q}_a\right]^T = \left[{}^I\mathbf{q}_{b,r} \;\; {}^I\mathbf{q}_{b,p} \;\; \mathbf{q}_a\right]^T \in \mathbb{R}^{6+n_a}. \tag{2}$$

The generalized velocity is expressed as follows:

$$\mathbf{u} = \left[{}^I\boldsymbol{\omega}_b \;\; {}^I\boldsymbol{\upsilon}_b \;\; \dot{\mathbf{q}}_a\right]^T \in \mathbb{R}^{6+n_a}. \tag{3}$$

The conversion relationship between generalized velocity and generalized variable differential is expressed as follows:

$$\mathbf{u} = \begin{bmatrix} \mathbf{R}_{rw} & 0 & 0 \\ 0 & \mathbf{I}_{3\times 3} & 0 \\ 0 & 0 & \mathbf{I}_{n_a\times n_a} \end{bmatrix} \cdot \dot{\mathbf{q}}, \tag{4}$$

where

$$\mathbf{R}_{r\omega} = \begin{bmatrix} \cos\left(q_{b,yaw}\right)\cos\left(q_{b,pitch}\right) & -\sin\left(q_{b,yaw}\right) & 0 \\ \sin\left(q_{b,yaw}\right)\cos\left(q_{b,pitch}\right) & \cos\left(q_{b,yaw}\right) & 0 \\ -\sin\left(q_{b,pitch}\right) & 0 & 1 \end{bmatrix}.$$

According to the posture transformation matrix of any point Q on the robot in the inertial system, the Jacobian

matrix of point Q in the inertial coordinate system can be obtained as follows:

$$
\begin{aligned}
{}^{I}\mathbf{J}_{IQ}(q) &= \begin{bmatrix} {}^{I}\mathbf{J}_{R} \\ {}^{I}\mathbf{J}_{P} \end{bmatrix} \\
&= \begin{bmatrix} \mathbf{I}_{3\times3} & \\ -{}^{I}\mathbf{R}_{IB}(q)\cdot\left[{}^{B}\mathbf{p}_{BQ}(q_a)\right]_{\times}\cdot{}^{I}\mathbf{R}_{IB}{}^{T}(q) & \\ \mathbf{0}_{3\times3} & {}^{I}\mathbf{R}_{IB}(q)\cdot{}^{B}\mathbf{J}_{R_{qa}}(q_a) \\ \mathbf{I}_{3\times3} & {}^{I}\mathbf{R}_{IB}(q)\cdot{}^{B}\mathbf{J}_{P_{qa}}(q_a) \end{bmatrix},
\end{aligned} \tag{5}
$$

where ${}^{I}\mathbf{R}_{IB}(q)$ is the posture transformation matrix of the robot base link under the inertial system, and ${}^{B}p_{BQ}(q_a)$ is the position of the point Q relative to the origin of base system under the base system, ${}^{B}\mathbf{J}_{R_{qa}}(q_a)$ and ${}^{B}\mathbf{J}_{P_{qa}}(q_a)$ are the angular and linear velocity Jacobian matrix of point Q under the base system, respectively.

According to the various mapping objects, the base task Jacobian, swing-leg task Jacobian and contact Jacobian are obtained as follows:

$$
{}^{I}\mathbf{J}_{IB\_task} = \begin{bmatrix} I_{3\times3} & 0_{3\times3} & 0_{3\times n_a} \\ 0_{3\times3} & I_{3\times3} & 0_{3\times n_a} \end{bmatrix}, \tag{6}
$$

$$
{}^{I}\mathbf{J}_{IF\_task} = \begin{bmatrix} \mathbf{I}_{3\times3} & \\ -{}^{I}\mathbf{R}_{IB}(q)\bullet\left[{}^{B}\mathbf{p}_{BF}(q_a)\right]_{\times}\bullet{}^{I}\mathbf{R}_{IB}{}^{T}(q) & \\ \mathbf{0}_{3\times3} & {}^{I}\mathbf{R}_{IB}(q)\bullet{}^{B}\mathbf{J}_{FR_{qa}}(q_a) \\ \mathbf{I}_{3\times3} & {}^{I}\mathbf{R}_{IB}(q)\bullet{}^{B}\mathbf{J}_{FP_{qa}}(q_a) \end{bmatrix}, \tag{7}
$$

$$
{}^{I}\mathbf{J}_{c} = \begin{bmatrix} \mathbf{I}_{3\times3} & \\ -{}^{I}\mathbf{R}_{IB}(q)\bullet\left[{}^{B}\mathbf{p}_{Bc}(q_a)\right]_{\times}\bullet{}^{I}\mathbf{R}_{IB}{}^{T}(q) & \\ \mathbf{0}_{3\times3} & {}^{I}\mathbf{R}_{IB}(q)\bullet{}^{B}\mathbf{J}_{cR_{qa}}(q_a) \\ \mathbf{I}_{3\times3} & {}^{I}\mathbf{R}_{IB}(q)\bullet{}^{B}\mathbf{J}_{cP_{qa}}(q_a) \end{bmatrix}. \tag{8}
$$

3.2. Dynamic model

Due to the floating base system, the whole-body dynamics model of the bipedal robot was established using the Lagrangian method as follows:

$$
\mathbf{M}\ddot{\mathbf{q}} + \mathbf{h} = \mathbf{S}^{T}\boldsymbol{\tau} + {}^{I}\mathbf{J}_{c}{}^{T}\mathbf{f}_{c}, \tag{9}
$$

where $\mathbf{M}$ is the inertia matrix of the floating base system, $\mathbf{h}$is the centrifugal force, coriolis force and gravity term. Furthermore $\mathbf{S}$ is the selection matrix of active joint, and $\boldsymbol{\tau}$ is the moment vector of active joints. Here, ${}^{I}\mathbf{J}_{c}$ is the contact Jacobian matrix, and $\mathbf{f}_c$ is the foot contact force spin exerted by the ground on the feet, $\mathbf{f}_c = [\tau_{yaw},\ f_x,\ f_y,\ f_z]^T$.

The model is then split into two parts, the floating base and leg, corresponding to nonactive and active parts

$$
\begin{aligned}
\mathbf{M}_b\bullet\dot{u} + \mathbf{h}_b &= {}^{I}\mathbf{J}_{cb}{}^{T}\bullet\mathbf{f}_c, \\
\mathbf{M}_a\bullet\dot{u} + \mathbf{h}_a &= \boldsymbol{\tau} + {}^{I}\mathbf{J}_{ca}{}^{T}\bullet\mathbf{f}_c.
\end{aligned} \tag{10}
$$

The equation indicates that the floating base part relies on the contact force spin from the ground to achieve movement, whereas the movement of leg part is the result of the active joint torque and contact force spin. The nonactive model contains a coupling term between the floating base and leg. After removing the term, the single rigid body dynamic model of floating base is obtained as follows:

$$
\begin{cases}
\dfrac{d}{dt}\left(\hat{\mathbf{I}}\bullet{}^{I}\omega_b\right) = \sum_i\left(\boldsymbol{\tau}_i + \left[{}^{I}\mathbf{p}_{Bc}(q)\right]_{\times}\bullet\mathbf{f}_i\right), \\
m\bullet{}^{I}\dot{v}_b + m\hat{\mathbf{g}} = \sum_i f_i,
\end{cases} \tag{11}
$$

where $\hat{\mathbf{I}}$ is the inertia moment of floating base in the inertial system, m is the mass of floating base, $\mathbf{f}_i$ and $\boldsymbol{\tau}_i$ are the foot contact forces and moments from the ground. Here, ${}^{I}\mathbf{p}_{Bc}(q)$ is the foot position relative to the origin of base system under the inertial system during the stand phase, and the direction is from the origin of base system to the foot, ${}^{I}\mathbf{R}_{IB}(q)\bullet\left[{}^{B}\mathbf{p}_{Bc}(q_a)\right]_{\times}\bullet{}^{I}\mathbf{R}_{IB}{}^{T}(q) = \left[{}^{I}\mathbf{p}_{Bc}(q)\right]_{\times}$. $\hat{\mathbf{g}} = \begin{bmatrix}0 & 0 & g\end{bmatrix}^{T}$ is the gravity acceleration vector.

4. CONTROL FRAMEWORK

Fig. 3 shows the proposed control framework for the high dynamic locomotion of bipedal robot. The operator provides the robot forward and lateral velocity $v_{b,x}$, $v_{b,y}$ and yaw rate $\omega_{b,z}$ through the manual remote control, and subsequently through the velocity integration to obtain the desired state $\mathbf{x}_d$ of the floating base. The state machine determines the contact event according to the estimated value of contact force, to obtain the controller and leg modes. Then values are introduced into the model predictive controller, the swing leg trajectory planner and task hierarchical optimization controller. The desired state $\mathbf{x}_d$ and the estimated value x of actual state are introduced into MPC to calculate the contact force spin of the stand leg. Simultaneously, the desired foot locations and trajectory planning of swing leg are calculated. These values are output to THOC in real time, to generate joint control torque to drive the robot to locomotion. The state estimation is obtained by the fusion of IMU acceleration and stand leg kinematics. However, this model is not the focus of this paper, and is not repeated here.

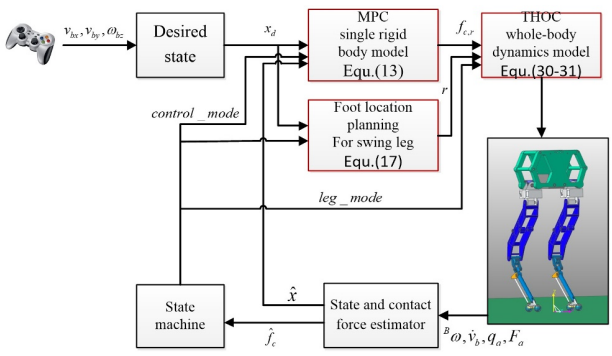

Fig. 3. The control framework.

The cascade control framework is composed of two layers: the upper layer is MPC based on a single rigid body model of floating base, and the lower layer is THOC based on the whole-body dynamics model.

a) In the upper layer, the under-actuated time-sharing control principle was used to divide a gait cycle into two parts: the stand and the swing phases. Corresponding to the bipedal robot studied, when one leg was in the stand phase, the MPC based on the single rigid body model was used to control the posture and height of the model, and the other leg was in the swing phase, and the foot locations is used to control the forward and lateral velocities of the robot. The desired force spin of the stand leg and the desired trajectory of swing leg were calculated and sent to the lower controller.

b) In the lower layer, tasks include whole-body dynamics constraints, nonslip feet constraints, pose control task, and torque minimum task. Based on the task hierarchical optimization controller, the active joint torque was optimally calculated. The framework ensured that the six DOFs of the robot are controllable in the time-sharing control, with the alternate movement of the left and right legs, the 3D locomotion and antidisturbance control were realized for the high-velocity dynamic of the bipedal robot with large inertia legs.

The single rigid body model is derived from the whole body dynamics ignoring the dynamic part of legs. Therefore, the contact force spin planned by MPC is not equal to that required by THOC and $\mathbf{f}_{c\_THOC}$ is generally greater than $\mathbf{f}_{c\_MPC}$. Therefore, a contact force relaxation variable $\triangle \mathbf{f}_c$ was designed to compensate for the difference between $\mathbf{f}_{c\_MPC}$ and $\mathbf{f}_{c\_THOC}$, and the relationship was $\mathbf{f}_{c\_THOC} = \mathbf{f}_{c\_MPC} + \triangle \mathbf{f}_c$. Thus, the relationship between MPC and THOC was developed. Because MPC provides a stable expected median for the contact force spin, based on minimizing the relaxation variable $\triangle \mathbf{f}_c$, $\mathbf{f}_{c\_THOC}$ approaches and tracks $\mathbf{f}_{c\_MPC}$ under the whole-body dynamics constraints, thus, the cascade controller with MPC and THOC was constructed.

5. CASCADE CONTROLLER VIA MPC AND THOC

5.1. MPC based on single rigid body model

According to (11), the discrete state equation of the single rigid body model for the floating base is as follows:

$$\mathbf{x}(k+1) = \mathbf{A}_k \cdot \mathbf{x}(k) + \mathbf{B}_k \cdot \mathbf{u}(k), \tag{12}$$

where $\triangle T$ is the discrete time step

$$\mathbf{x}(k) = \left[{}^I\mathbf{q}_{b,r},\ {}^I\mathbf{q}_{b,p},\ {}^I\boldsymbol{\omega}_b,\ {}^I\upsilon_b,\ \mathbf{g}\right]^T,$$

$$\mathbf{u}(k) = \mathbf{f}_{c\_MPC} = \left[\widehat{\mathbf{f}}_{c,L},\ \widehat{\mathbf{f}}_{c,R}\right]^T,$$

$$\mathbf{A}_k = \begin{bmatrix} \mathbf{1}_{3\times3} & \mathbf{0}_{3\times3} & \triangle T\cdot\mathbf{R}_{\omega r} & \mathbf{0}_{3\times3} & \mathbf{0}_{3\times3} \\ \mathbf{0}_{3\times3} & \mathbf{1}_{3\times3} & \mathbf{0}_{3\times3} & \triangle T\cdot\mathbf{1}_{3\times3} & \mathbf{0}_{3\times3} \\ \mathbf{0}_{3\times3} & \mathbf{0}_{3\times3} & \mathbf{1}_{3\times3} & \mathbf{0}_{3\times3} & \mathbf{0}_{3\times3} \\ \mathbf{0}_{3\times3} & \mathbf{0}_{3\times3} & \mathbf{0}_{3\times3} & \mathbf{1}_{3\times3} & \triangle T\cdot\mathbf{k}_g \\ \mathbf{0}_{3\times3} & \mathbf{0}_{3\times3} & \mathbf{0}_{3\times3} & \mathbf{0}_{3\times3} & 1 \end{bmatrix},$$

$$\mathbf{B}_k = \begin{bmatrix} \mathbf{0}_{3\times1} & \mathbf{0}_{3\times3} & \mathbf{0}_{3\times1} & \mathbf{0}_{3\times3} \\ \mathbf{0}_{3\times1} & \mathbf{0}_{3\times3} & \mathbf{0}_{3\times1} & \mathbf{0}_{3\times3} \\ \frac{k_\tau}{\hat{\mathbf{I}}} & \frac{\left[{}^I\mathbf{p}_{Bc,L}(q)\right]_\times}{\hat{\mathbf{I}}} & \frac{k_\tau}{\hat{\mathbf{I}}} & \frac{\left[{}^I\mathbf{p}_{Bc,R}(q)\right]_\times}{\hat{\mathbf{I}}} \\ \mathbf{0}_{3\times1} & \mathbf{1}_{3\times3}/m & \mathbf{0}_{3\times1} & \mathbf{1}_{3\times3}/m \\ 0 & \mathbf{0}_{1\times3} & 0 & \mathbf{0}_{1\times3} \end{bmatrix},$$

$$\widehat{\mathbf{f}}_{c,L} = \left[\tau_{yaw,L},\ f_{x,L},\ f_{y,L},\ f_{z,L}\right]^T,$$

$$\widehat{\mathbf{f}}_{c,R} = \left[\tau_{yaw,R},\ f_{x,R},\ f_{y,R},\ f_{z,R}\right]^T,$$

$$\mathbf{R}_{\omega r} = \begin{bmatrix} \cos(q_{b,yaw})/\cos(q_{b,pitch}) & 0 \\ -\sin(q_{b,yaw}) & 0 \\ \cos(q_{b,yaw})\tan(q_{b,pitch}) & 1 \end{bmatrix}.$$

To track the desired trajectory, a cost function was designed to reflect the performance of control system. The cost function contains the following two items: the first item is to minimize the tracking error of state trajectory, the second item is to minimize the control sequence, and the optimized variable is the contact force spin $\mathbf{u} = \mathbf{f}_{c\_mpc}$. Next, dynamic and physical constraints are added, and the optimization problem of trajectory tracking is constructed as follows:

$$\min_u \sum_{i=1}^{N_p} \left\|\mathbf{x}(k+i\mid t) - \mathbf{x}_{ref}(k+i\mid t)\right\|_{\mathbf{Q}}^2 + \sum_{i=0}^{N_c-1} \left\|\mathbf{u}(k+i\mid t)\right\|_{\mathbf{R}}^2, \tag{13a}$$

s.t.

$$\mathbf{x}(k+i\mid t) = \mathbf{A}_{k,t}\cdot\mathbf{x}(k+i-1\mid t) + \mathbf{B}_{k,t}\cdot\mathbf{u}(k+i-1\mid t), \tag{13b}$$

$$\underline{\mathbf{c}}_i \le \mathbf{C}_i\mathbf{u}(k+i-1) \le \bar{\mathbf{c}}_i, \tag{13c}$$

$$\mathbf{D}_i\mathbf{u}(k+i-1) = \mathbf{0},\ i = 1,\ \ldots,\ N_p, \tag{13d}$$

where (13b) is the dynamic constraint, and (13c) is the inequality constraint, which includes the friction cone constraint (see (14)). Equation (13d) is the equality constraint, which integrates the gait sequence into the optimization solution by selecting the foot contact force torque (see (15) for details). Based on (11), the MPC optimization problem (13a) is transformed into a linear quadratic programming problem (QP) standard form, and the contact force spin $\mathbf{f}_{c\_mpc}$ is calculated by optimizing the solution during the control period.

Here N_p is the prediction step, N_c is the control step, i is the step i, k is the moment k, $\mathbf{Q}$ and $\mathbf{R}$ are weight matrices of state and control, respectively.

For the bipedal robot under consideration, only four active joints were present in a single leg. Therefore, corresponding to the two degrees of freedom x and y, the gain values in the weight matrix $\mathbf{Q}$ were set to zero in the MPC controller, which relinquishes the control of these two DOFs during the stand phase.

a) Friction cone constraint

During the contact between the foot and ground, the ground only exerts a ground reaction force on the foot and cannot form a pulling force. Therefore, contact force f_z in the vertical direction should be greater than or equal to zero. Considering that the ground is uneven, the component of the contact force in the normal direction of ground is greater than or equal to zero. In addition, limited by the maximum drive capacity of joint driver, the contact force has a maximum value.

$$\begin{aligned} &\widehat{\mathbf{f}}_c \bullet \hat{\mathbf{n}} \geq 0, \\ &f_z \leq f_{z,\max}, \end{aligned} \tag{14a}$$

where $\hat{\mathbf{n}}$ is the normal vector of the contact position between foot and ground, $\widehat{\mathbf{f}}_c$ is contact force relaxation and f_z is the foot force in the vertical direction.

To prevent an uncontrollable state caused by foot slipping, the contact force in the forward and lateral directions is limited to the range of the friction cone as follows:

$$\begin{aligned} &-\mu f_z \leq f_x \leq \mu f_z, \\ &-\mu f_z \leq f_y \leq \mu f_z, \end{aligned} \tag{14b}$$

where μ refers to the friction coefficient, f_x refers to the foot force in the horizontal direction, and f_y refers to the foot force in the lateral direction.

The contact yaw moment forms a lateral force at the front and rear contact points, which is superimposed on the lateral contact force, as shown in Fig. 2 (blue arrow). Therefore, this value should be limited to the friction cone range

$$\begin{aligned} &-\mu f_z \leq (\tau_{yaw}/L_{toe} + f_y) \leq \mu f_z, \\ &-\mu f_z \leq (-\tau_{yaw}/L_{heel} + f_y) \leq \mu f_z, \end{aligned} \tag{14c}$$

where L_{toe} and L_{heel} are the distances from the projection point of ankle joint on the ground to the two front and back contact points, respectively, and τ_{yaw} refers to the moment in the yaw direction.

b) Gait constraint

When the leg is in the swing phase, the equation constraint is used to force the contact force spin of the leg to zero; when the leg is in the stand phase, the contact force spin is not constrained at this stage, and is calculated by other constraints. After unifying the left and right legs into a frame, an 8×8 dimension matrix was obtained. When the left leg is supported and right leg is swinging, the equation constraint is expressed as follows:

$$\underbrace{\begin{bmatrix} \mathbf{0}_{4\times4} & \\ & \mathbf{1}_{4\times4} \end{bmatrix}}_{\mathbf{D}_i} \cdot \mathbf{u}(k+i-1) = \begin{bmatrix} \mathbf{0}_{4\times1} \\ \mathbf{0}_{4\times1} \end{bmatrix}. \tag{15a}$$

When the right leg is supported and left leg is swinging, the equation constraint changes to the following:

$$\underbrace{\begin{bmatrix} \mathbf{1}_{4\times4} & \\ & \mathbf{0}_{4\times4} \end{bmatrix}}_{\mathbf{D}_i} \cdot \mathbf{u}(k+i-1) = \begin{bmatrix} \mathbf{0}_{4\times1} \\ \mathbf{0}_{4\times1} \end{bmatrix}. \tag{15b}$$

The solution process of MPC based on single rigid body model (13).

1) Prediction model

The N_p step state prediction matrix form of dynamic model (12) is obtained by iterative calculation

$$\mathbf{X}(t) = \mathbf{\Psi}_t \mathbf{x}(k \mid t) + \mathbf{\Theta}_t \mathbf{U}(t), \tag{16a}$$

$$\mathbf{X}(t) = \begin{bmatrix} \mathbf{x}(k+1 \mid t) \\ \mathbf{x}(k+2 \mid t) \\ \vdots \\ \mathbf{x}(k+N_p \mid t) \end{bmatrix}, \mathbf{\Psi}_t = \begin{bmatrix} \mathbf{A}_{k,t} \\ \mathbf{A}_{k+1,t}\mathbf{A}_{k,t} \\ \vdots \\ \prod_{i=k}^{k+N_p-1} \mathbf{A}_{i,t} \end{bmatrix},$$

$$\mathbf{U}(t) = \begin{bmatrix} \mathbf{u}(k \mid t) \\ \mathbf{u}(k+1 \mid t) \\ \vdots \\ \mathbf{u}(k+N_c \mid t) \end{bmatrix},$$

$$\mathbf{\Theta}_t = \begin{bmatrix} \mathbf{B}_{k,t} & \mathbf{0}_{N_p\times N_u} & \mathbf{0}_{N_p\times N_u} \\ \mathbf{A}_{k+1,t}\mathbf{B}_{k,t} & \mathbf{B}_{k+1,t} & \mathbf{0}_{N_p\times N_u} \\ \vdots & \vdots & \ddots \\ \prod_{i=k+1}^{k+N_p-1} \mathbf{A}_{i,t}\mathbf{B}_{k,t} & \prod_{i=k+2}^{k+N_p-1} \mathbf{A}_{i,t}\mathbf{B}_{k+1,t} & \cdots \\ & \mathbf{0}_{N_p\times N_u} & \\ & \mathbf{0}_{N_p\times N_u} & \\ & \vdots & \\ & \prod_{i=k+N_c}^{k+N_p-1} \mathbf{A}_{i,t}\mathbf{B}_{k+N_c-1,t} & \end{bmatrix}.$$

2) Horizon optimization

Based on the aforementioned prediction model, the MPC optimization problem (13a) was transformed into the linear QP.

$$\min_{\mathbf{U}(t)} \mathbf{U}(t)^T \mathbf{H} \mathbf{U}(t) + \mathbf{G}^T \mathbf{U}(t), \tag{16b}$$

where

$$\mathbf{H} = \mathbf{\Theta}_t^T \mathbf{Q} \mathbf{\Theta}_t + \mathbf{R},\ \mathbf{G} = 2\mathbf{\Theta}_t^T \mathbf{Q} \left(\mathbf{\Psi}_t \mathbf{x}(k \mid t) - \mathbf{X}_{ref}(t) \right).$$

$\mathbf{X}_{ref}(t)$ is the desired trajectory of N_p steps, which is obtained by integral accumulation iteration according to desired state and velocity at the current moment. The constraint matrix is expanded on the single step constraint dimension to obtain the dimension corresponding to the prediction model.

The dimension of one-step constraint is extended N_p times to obtain the dimension of constraint matrix corresponding to the prediction model. Inequality constraint (14) is transformed into $\mathbf{A} \bullet \mathbf{U}(t) \leq \mathbf{b}$, and equality constraint (15) corresponds to $\mathbf{A}_{eq} \bullet \mathbf{U}(t) = \mathbf{b}_{eq}$. Thus, the standard linear quadratic programming form is constructed

$$\min_{U(t)} \mathbf{U}(t)^T \mathbf{H} \mathbf{U}(t) + \mathbf{G}^T \mathbf{U}(t), \tag{16c}$$

s.t.

$$\mathbf{A} \bullet \mathbf{U}(t) \leq \mathbf{b},$$
$$\mathbf{A}_{eq} \bullet \mathbf{U}(t) = \mathbf{b}_{eq}.$$

3) Feedback compensation

Given the real-time state $\mathbf{x}(k \mid t)$ at time k, the quadprog function was used to solve the standard linear quadratic programming in the control period, and the control sequence $\mathbf{U}^*(t)$ was obtained. The first quantity of this sequence was considered as actual control quantity.

$$\mathbf{f}_{c\_MPC} = \mathbf{u}(k) = [1,\ 0,\ \ldots]_{1 \times N_c} \cdot \mathbf{U}^*(t). \tag{16d}$$

5.2. Foot location planning for the swing leg

First, the desired foot location is calculated, and to lift the legs at a certain height and smooth transition, the swing leg trajectory is planned online. The foot location of swing leg in the inertial system is expressed as follows:

$$\begin{aligned} \mathbf{p}_{\mathrm{f,des}} = \mathbf{p}_{com} + \mathbf{R}_{IB}{}^{B}\mathbf{p}_{B\_hip} + \frac{t_{stance}}{2}{}^{I}\mathbf{v}_b \\ + \mathbf{k}\left({}^{I}\mathbf{v}_b - {}^{I}\mathbf{v}_{b,des}\right) + \frac{1}{2}\sqrt{{}^{I}\mathbf{q}_{b,pz}/g} \bullet {}^{I}\mathbf{v}_b \times {}^{I}\boldsymbol{\omega}_{bz,des}, \end{aligned} \tag{17}$$

where the first term $\mathbf{p}_{com}$ is the real-time position of the floating base in the inertial system, the second term $\mathbf{R}_{IB}{}^{B}\mathbf{p}_{B\_hip}$ is the position from the base system to the hip under the inertial system, and the third and fourth terms are the Raibert heuristic. Here ${}^{I}\mathbf{v}_b = \left[{}^{I}v_{bx},\ {}^{I}v_{by},\ 0\right]^T$ denotes the robot actual velocities in the inertial system, and correspondingly, ${}^{I}\mathbf{v}_{b,des} = \left[{}^{I}v_{bx,des},\ {}^{I}v_{by,des},\ 0\right]^T$ denotes the desired velocities. The fifth item is the foot compensation item during yaw, where ${}^{I}\mathbf{q}_{b,pz}$ is the height of the robot and ${}^{I}\boldsymbol{\omega}_{bz,des}$ is the desired yaw velocity. By using this equation, the foot location in the x and y directions was obtained under the inertial system. Based on the standing plane, the foot location in the z direction was descended 10 mm to ensure that the foot touches the ground slightly in advance.

Considering the smooth trajectory, the swing leg trajectory adopts a third-order Bezier curve, the form of which is presented in (18). According to a fixed time period, the curve trajectory is determined by four control points, namely starting point $\mathbf{p}_0$, middle control point $\mathbf{p}_1$, the middle control point $\mathbf{p}_2$ and the foot location point $\mathbf{p}_d = \mathbf{p}_{\mathrm{f,des}}$. All of these four points should be in the reachable space.

$$\begin{aligned} \mathbf{x}_{d\_f} = (1-m)^3\mathbf{p}_0 + 3m(1-m)^2\mathbf{p}_1 \\ + 3m^2(1-m)\mathbf{p}_2 + m^3\mathbf{p}_d, \end{aligned} \tag{18}$$

where $m \in \begin{bmatrix} 0 & 1 \end{bmatrix}$ is the normalized amount of time. The planned swing leg trajectory $\mathbf{x}_{d\_f}$ is differentiated to obtain the desired velocity $\dot{\mathbf{x}}_{d\_f}$ and acceleration $\ddot{\mathbf{x}}_{d\_f}$. To provide stable support for the robot and avoid sliding and impact, swinging the leg fast lifting and slowly touching the ground are critical. Therefore, two middle control points are set as follows:

$$\begin{aligned} p_1 &= \left[p_{0,1} + (p_{d,1} - p_{0,1})/2,\ p_{0,2} + (p_{d,2} - p_{0,2})/2,\right. \\ &\quad \left. p_{0,3} + H\right]^T, \\ p_2 &= \left[p_{d,1},\ p_{d,2},\ p_{0,3} + H\right]^T, \end{aligned}$$

H is leg lift height.

5.3. Task hierarchical optimization controller based on the whole-body dynamics model

Task hierarchical optimization controller was used to satisfy the whole-body dynamics constraint task, the other tasks are then sorted by priority, and finally the optimization solution is executed in a specific order, such that the solution of low-priority task should satisfy high-priority tasks. In the optimization solution of each task, at the outer loop level, the corresponding space (operation/joint space) controller is designed, and at the inner loop level, the trajectory tracking optimization controller is designed under the constraints of equations and inequalities. Using generalized acceleration and contact force compensation as optimization variables $\bar{\mathbf{X}} = [\ddot{\mathbf{q}},\ \triangle\ \mathbf{f}_c]^T$, the controller is described in detail as follows:

1) Task priority and outer loop controller

a) First priority task (Dynamic constraints): The whole-body dynamics model of the robot is expressed as follows:

$$\mathbf{M}\ddot{\mathbf{q}} + \mathbf{h} = \mathbf{S}^T\boldsymbol{\tau} + {}^{I}\mathbf{J}_c{}^T\left(\mathbf{f}_{c\_mpc} + \triangle\ \mathbf{f}_c\right). \tag{19}$$

To correspond to the optimized variables, the following nonactive part model is considered

$$\mathbf{M}_b\ddot{\mathbf{q}} + \mathbf{h}_b = {}^{I}\mathbf{J}_{cb}{}^T\left(\mathbf{f}_{c\_mpc} + \triangle\ \mathbf{f}_c\right). \tag{20}$$

Constructed as a function with optimized variables, we have the following expression

$$\underbrace{\begin{bmatrix}\mathbf{M}_b & -{}^{I}\mathbf{J}_{cb}{}^T\end{bmatrix}}_{\mathbf{A}_1}\begin{bmatrix}\ddot{\mathbf{q}} \\ \triangle\ \mathbf{f}_c\end{bmatrix} = \underbrace{{}^{I}\mathbf{J}_{cb}{}^T \cdot \mathbf{f}_{c\_mpc} - \mathbf{h}_b}_{\mathbf{b}_1}, \tag{21}$$

where subscripts $\mathbf{A}_1$ and $\mathbf{b}_1$ are used to in the design of cost function in the algorithm.

b) The second priority task (Foot contact nonslip constraint):

$$ {}^{I}\mathbf{J}_c\ddot{\mathbf{q}} + {}^{I}\dot{\mathbf{J}}_c\dot{\mathbf{q}} = \ddot{\mathbf{x}}_c = 0, \tag{22} $$

$$ \underbrace{\begin{bmatrix} {}^{I}\mathbf{J}_c & \mathbf{0} \end{bmatrix}}_{\mathbf{A}_2} \begin{bmatrix} \ddot{\mathbf{q}} \\ \triangle \mathbf{f}_c \end{bmatrix} = \underbrace{-{}^{I}\dot{\mathbf{J}}_c\dot{\mathbf{q}}}_{\mathbf{b}_2}. \tag{23} $$

c) The third priority task (The posture and height of floating base): The desired values of posture and height are consistent with the desired values in MPC. The outer loop controller is expressed as follows:

$$ \ddot{\mathbf{x}}_{cmd\_b} = \ddot{\mathbf{x}}_{d\_b} + \mathbf{k}_{p\_b}(\mathbf{x}_{d\_b} - \mathbf{x}_b) + \mathbf{k}_{d\_b}(\dot{\mathbf{x}}_{d\_b} - \dot{\mathbf{x}}_b). \tag{24} $$

Constructed as a function with optimized variables, we have the following expression

$$ \underbrace{\begin{bmatrix} {}^{I}\mathbf{J}_{IB\_task} & \mathbf{0} \end{bmatrix}}_{\mathbf{A}_3} \begin{bmatrix} \ddot{\mathbf{q}} \\ \triangle \mathbf{f}_c \end{bmatrix} = \underbrace{\ddot{\mathbf{x}}_{cmd\_b} - {}^{I}\dot{\mathbf{J}}_{IB\_task} \cdot \dot{\mathbf{q}}}_{\mathbf{b}_3}, \tag{25} $$

where $\mathbf{x}_{d\_b}$, $\dot{\mathbf{x}}_{d\_b}$ and $\ddot{\mathbf{x}}_{d\_b}$ are the desired position, velocity and acceleration trajectory of the attitude and height for the floating base, respectively, $\ddot{\mathbf{x}}_{cmd\_b}$ is the control value calculated by the feedback control, $\mathbf{x}_b$ and $\dot{\mathbf{x}}_b$ are the real state, $\mathbf{k}_{p\_b}$ and $\mathbf{k}_{d\_b}$ are the diagonal gain matrix for controller. Here ${}^{I}\dot{\mathbf{J}}_{IB\_task}$ is the derivative of the Jacobian matrix ${}^{I}\mathbf{J}_{IB\_task}$.

d) The fourth priority task (The pose of swing leg): The outer loop controller is

$$ \ddot{\mathbf{x}}_{cmd\_f} = \ddot{\mathbf{x}}_{d\_f} + \mathbf{k}_{p\_f}(\mathbf{x}_{d\_f} - \mathbf{x}_f) + \mathbf{k}_{d\_f}(\dot{\mathbf{x}}_{d\_f} - \dot{\mathbf{x}}_f). \tag{26} $$

Constructed as a function with optimized variables

$$ \underbrace{\begin{bmatrix} {}^{I}\mathbf{J}_{IF\_task} & \mathbf{0} \end{bmatrix}}_{\mathbf{A}_4} \begin{bmatrix} \ddot{\mathbf{q}} \\ \triangle \mathbf{f}_c \end{bmatrix} = \underbrace{\ddot{\mathbf{x}}_{cmd\_f} - {}^{I}\dot{\mathbf{J}}_{IF\_task} \cdot \dot{\mathbf{q}}}_{\mathbf{b}_4}, \tag{27} $$

where $\mathbf{x}_{d\_f}$, $\dot{\mathbf{x}}_{d\_f}$ and $\ddot{\mathbf{x}}_{d\_f}$ are the desired position, velocity and acceleration trajectory for the pose of swing leg, respectively, $\ddot{\mathbf{x}}_{cmd\_f}$ is the control value calculated by the feedback control, $\mathbf{x}_f$ and $\dot{\mathbf{x}}_f$ are the real state, $\mathbf{k}_{p\_f}$ and $\mathbf{k}_{d\_f}$ are the diagonal gain matrix for the controller. Furthermore ${}^{I}\dot{\mathbf{J}}_{IF\_task}$ is the derivative of the Jacobian matrix ${}^{I}\mathbf{J}_{IF\_task}$.

e) The fifth priority task (Minimum joint torque): According to the active part of the whole-body dynamics, we have the following expression

$$ \mathbf{M}_a\ddot{\mathbf{q}} + \mathbf{h}_a = \boldsymbol{\tau} + {}^{I}\mathbf{J}_{ca}{}^{T}(\mathbf{f}_{c\_mpc} + \triangle \mathbf{f}_c). \tag{28} $$

Expect the joint torque $\boldsymbol{\tau}$ to approach 0 and construct a function with optimized variables as follows:

$$ \underbrace{\begin{bmatrix} \mathbf{M}_a & -{}^{I}\mathbf{J}_{ca}{}^{T} \end{bmatrix}}_{\mathbf{A}_5} \begin{bmatrix} \ddot{\mathbf{q}} \\ \triangle \mathbf{f}_c \end{bmatrix} = \underbrace{{}^{I}\mathbf{J}_{ca}{}^{T} \bullet \mathbf{f}_{c\_mpc} - \mathbf{h}_a}_{\mathbf{b}_5}. \tag{29} $$

f) The sixth priority task (Minimum contact force compensation): Expect the contact force compensation $\triangle \mathbf{f}_c$ to approach 0 and construct a function with optimized variables as follows:

$$ \underbrace{\begin{bmatrix} \mathbf{0} & \mathbf{I} \end{bmatrix}}_{\mathbf{A}_6} \begin{bmatrix} \ddot{\mathbf{q}} \\ \triangle \mathbf{f}_c \end{bmatrix} = \underbrace{\mathbf{0}}_{\mathbf{b}_6}, \tag{30} $$

where $\mathbf{I}$ is the inertia matrix of the floating base.

2) Task hierarchical optimization

Based on the forementioned task priorities, the hierarchical optimization algorithm is designed as follows:

$$ \min_{\ddot{q}, f_c} \mathbf{A}_i\bar{X}_i - \mathbf{b}_i, \tag{31a} $$

s.t.

$$ \mathbf{A}_j\bar{\mathbf{X}}_j{}^{*} = \mathbf{A}_j\bar{\mathbf{X}}_i,\ \forall j < i, \tag{31b} $$

$$ \boldsymbol{\tau}_{\min} \le \boldsymbol{\tau} \le \boldsymbol{\tau}_{\max}, \tag{31c} $$

$$ \mathbf{U} \cdot {}^{I}\mathbf{J}_c \le 0. \tag{31d} $$

The algorithm performs optimization calculations sequentially from the a) to f) tasks in the order of priority, which should satisfy the equality and inequality constraints of (31b)-(31d). The physical meaning of equality constraint (31b) is that the $\mathbf{A}_j\bar{\mathbf{X}}_i$ of i-th priority task should be equal to the $\mathbf{A}_j\bar{\mathbf{X}}_j{}^{*}$ of previous $(i-1)$-th, respectively. The purpose of equation constraint is to ensure the solution of the i-th priority task does not affect the control goal corresponding to the solution of previous $(i-1)$ high-priority tasks, and achieve strict priority stratification. Inequality constraints (31c) and (31d) are joint torque constraints and friction cone constraints, respectively.

The detailed calculation process of the hierarchical optimization algorithm (31) is as follows:

1) Define a) to f) tasks vector (21)-(29)
   $\mathbf{A} = [\mathbf{A}_a, \mathbf{A}_b, \mathbf{A}_c, \mathbf{A}_d, \mathbf{A}_e, \mathbf{A}_f]$,
   $\mathbf{b} = [\mathbf{b}_a, \mathbf{b}_b, \mathbf{b}_c, \mathbf{b}_d, \mathbf{b}_e, \mathbf{b}_f]$.
2) Define inequality constraints vector (31c)-(31d)
   $\mathbf{C} = [\mathbf{C}_{\tau\_up}, \mathbf{C}_{\tau\_low}, \mathbf{C}_{\lambda}]^T$,
   $\mathbf{D} = [\mathbf{d}_{\tau\_up}, \mathbf{d}_{\tau\_low}, \mathbf{d}_{\lambda}]^T$.
3) Initial equality constraints (31b)
   $\mathbf{A}_{eq} = [\,]$, $\mathbf{b}_{eq} = [\,]$;
   Num Tasks = length(A);

4) for $k = 1$: Num Tasks

$\mathbf{A}_i = \mathbf{A}(k)$, $\mathbf{b}_i = \mathbf{b}(k)$;;

$\mathbf{H} = \mathbf{A}_i^{'} \bullet \mathbf{A}_i$, $\mathbf{f} = -\mathbf{A}_i^{'} \bullet \mathbf{b}_i$;

$\mathbf{x} = \text{quadprog}(\mathbf{H}, \mathbf{f}, \mathbf{C}, \mathbf{D}, \mathbf{A}_{eq}, \mathbf{b}_{eq})$

Iteratively add equality constraints (31b)

$\mathbf{A}_{eq} = [\mathbf{A}_{eq}, \mathbf{A}_i]^T$; $\mathbf{b}_{eq} = [\mathbf{b}_{eq}, \mathbf{A}_i \bullet \mathbf{x}]$;

end

5) The hierarchical optimization solution (31a)

$\bar{X} = [\ddot{q}, \triangle f_c]^T = \mathbf{x}$.

After the optimization problem is solved and the optimized solution is obtained, the dynamic decomposition model is used to calculate the active joint torque as follows:

$$\boldsymbol{\tau} = \mathbf{M}_a \ddot{\mathbf{q}} - {}^{I}\mathbf{J}_{ca}{}^{T} \bullet (\mathbf{f}_{c\_mpc} + \triangle \mathbf{f}_c) + \mathbf{h}_a. \tag{32}$$

6. SIMULATION EXPERIMENT VERIFICATION OF HIGH DYNAMIC ANTI-INTERFERENCE PERFORMANCE

To verify the proposed dynamic antidisturbance performance of the cascade control framework, the multibody dynamics virtual prototype analysis software RecurDyn and the mathematical calculation software MATLAB were used to develop a bipedal robot multibody dynamics simulation platform.

The control parameters were set as follows: the control frequency of MPC was 100 Hz, and the weight was set to $\mathbf{Q} = diag([3e^6, 3e^6, 1e^7, 0, 0, 1e^9, 1e^3, 1e^3, 1e^4, 0, 0, 1e^6, 0])$, $\mathbf{R} = 0.1 \times diag([1, 1, 1, 1, 1, 1, 1, 1])$, The predicted horizon is $N_p = 3$, and control horizon is $N_c = 1$. Setting a smaller number of horizon is used to reduce the matrix dimension and improve the calculation velocity. In the state machine, the longest swing period was set to 0.25 s, the step height of swing leg was 0.15 m. In the friction cone constraint, the maximum foot force was 600 N in the z-axis and the friction coefficient was 0.6. The robot model parameters are presented in Table 1.

The control frequency of THOC is 500 Hz. Regarding the floating base task, the posture PD gains are $\mathbf{K}_{p\_pos} = 20 \cdot diag([3,\ 3,\ 1])$, $\mathbf{K}_{d\_\text{pos}} = 2 \bullet diag([3,\ 3,\ 1])$, which correspond to the roll, pitch, and yaw angle. The height PD gains are $K_{p\_h} = 300$, $K_{d\_body} = 30$. The PD gains for swing leg task are $\mathbf{K}_{p\_swing} = 5 \cdot diag([1,\ 1,\ 1,\ 7])$, $\mathbf{K}_{d\_\text{swing}} = 0.5 \cdot diag([1,\ 1,\ 1,\ 7])$. Because the objective of designing the algorithm is to improve the high dynamic locomotion velocity and antidisturbance ability of the robot, two cases of simulation experiments were performed. Namely, A) high-velocity forward experiment under walking gait and B) stable locomotion experiment under external interference.

Case A) (High-velocity forward experiment under walking gait)**:** A polynomial fitting method was used to draw up a smooth forward velocity desired trajectory, in which the transition time from zero to the maximum velocity was 15 s and the maximum desired velocity was 2.5 m/s. The desired forward position was obtained using the integral of velocity. The height of the floating base was set to 0.75 m, and other desired states were set to zeros. High-velocity motion simulation experiments were performed on flat ground, and the high dynamic locomotion process diagram is shown in Fig. 4. The contact force and moment curves in the z-axial direction are illustrated in Fig. 5. The Euler angle and position tracking curves of floating base are illustrated in Figs. 6 and 7, and the velocity tracking curves in x and y axis are shown in Fig. 8. Figs. 5-8 present detailed views between 15 and 16 s.

Figs. 7 and 8 present a comparison of height and velocity tracking effects between VMC based on decoupling idea [1], linear MPC (LMPC) based on linearized single rigid body model [28], nonlinear model predictive control (NMPC (SLQ-MPC)) based on nonlinear single

Table 1. Parameters.

Parameter	Symbol	Value	Units
Floating base quality	m	31.18	kg
Floating base inertia	I_{xx}	0.2843	kg·m^2
	I_{yy}	0.4142	kg·m^2
	I_{zz}	0.4432	kg·m^2
Hip position	l, w, h	(0, 0.12, 0.07)	m
Hip link length	L_2	0.15	m
Thigh link length	L_3	0.4	m
Calf link length	L_4	0.355	m

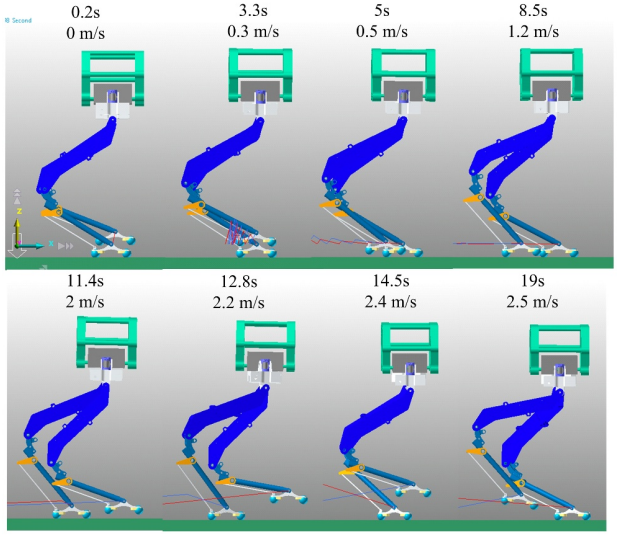

Fig. 4. High dynamic locomotion process diagram.

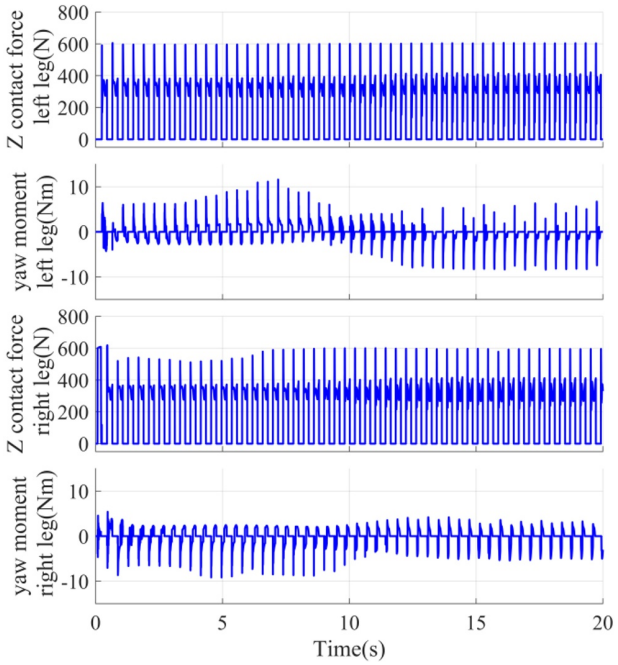

(a)

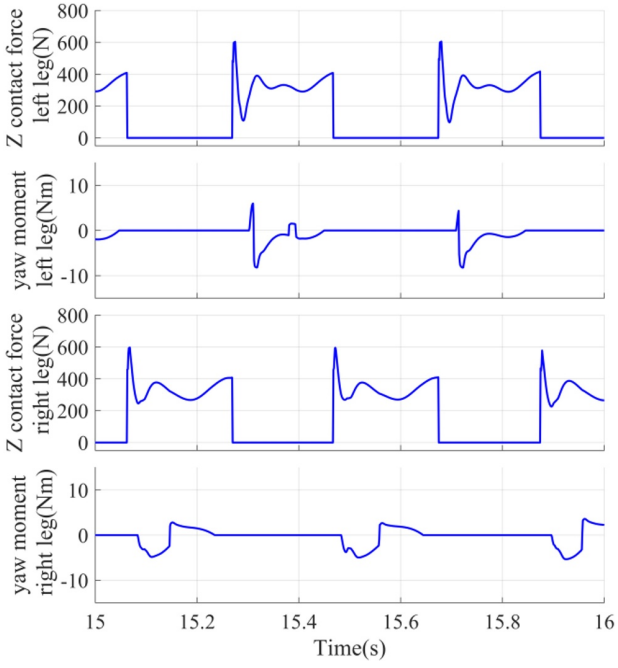

(b)

Fig. 5. Contact force and moment curves in the z-axial.

rigid body model [29] and the proposed algorithm (MPC-THOC).

Performance evaluation: The contact force of the z-axis in Fig. 5 reveals that from 10 to 15 s, when the velocity is increased from 1.8 to 2.5 m/s, the contact force increases in the stand phase, and the change trend reveals that the controller provides a force spin compatible with

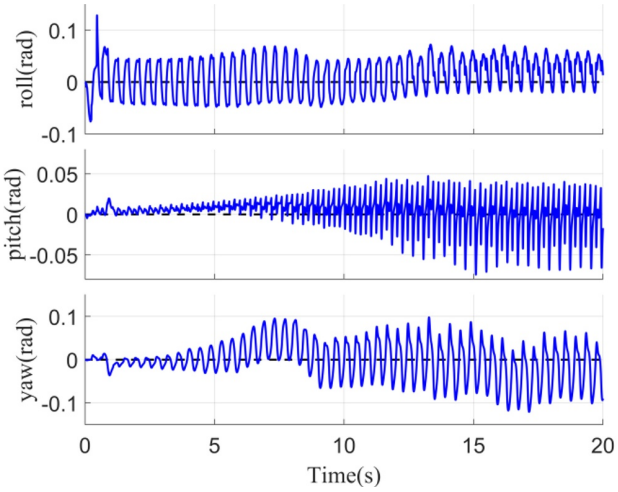

(a)

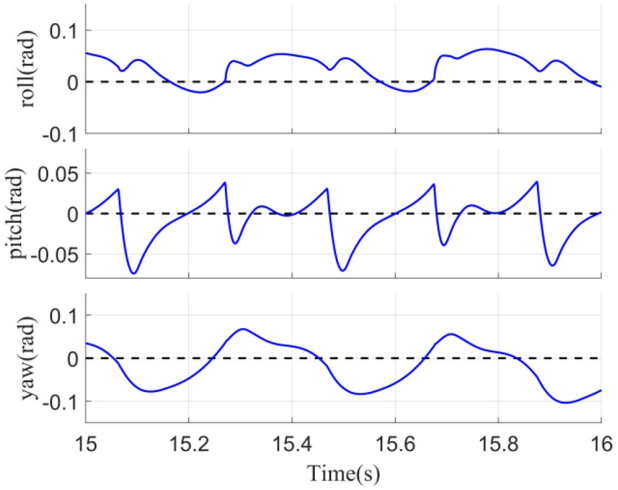

(b)

Fig. 6. Euler angle tracking curves of floating base.

the forward speed to control the posture and height of robot. As the Euler angle trajectory in Fig. 6, because of the forward motion, the roll angle is uniformly controlled within the range of ± 0.05 rad. The pitch and yaw angle revealed a constant increase in the velocity stage from 0-2.5 m/s. When the speed stabilized at 2.5 m/s, the two angles fluctuated steadily periodically with a finite amplitude between -0.08 to 0.05 rad and -0.11 to 0.1 rad with gait switching.

Figs. 7 and 8 reveal that compared with the 1.4 m/s of VMC,1.9 m/s of LMPC, and 2.15 m/s of NMPC, the robot maximum forward velocity reached 2.5 m/s under the cascade control framework (MPC-THOC), and the forward position and velocity trajectory were tracked accurately on the desired trajectory. The task hierarchical optimization controller and whole-body dynamic model helped in the stability control of pose and improved the dynamic velocity and antidisturbance robustness of the robot. In terms

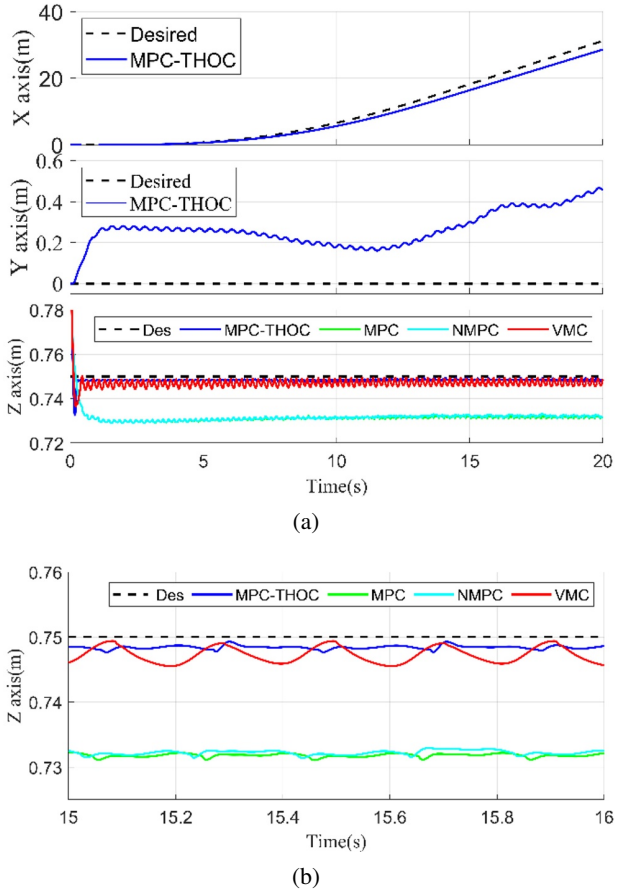

Fig. 7. The position tracking curves of floating base.

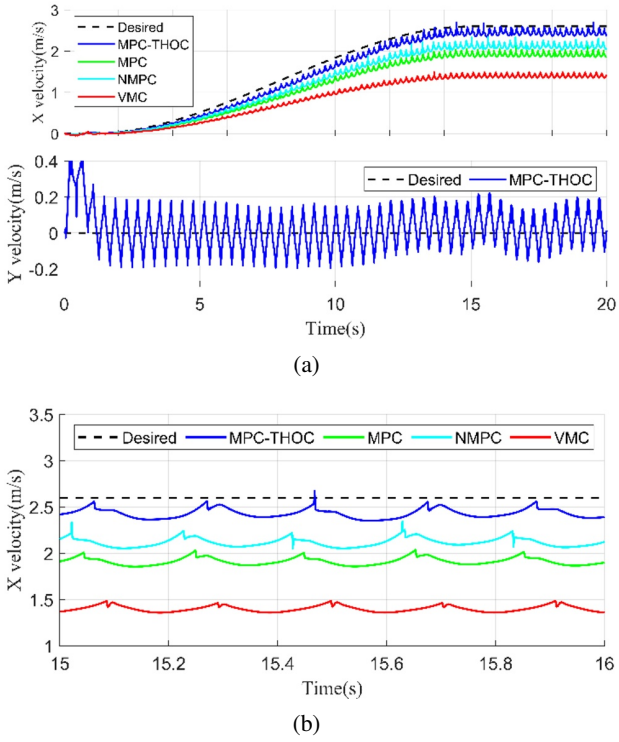

Fig. 8. The velocity tracking curves in x and y axis.

of lateral position and velocity, because of the robot moving under high dynamics, the lateral velocity control exhibited a certain offset, and the lateral displacement was slowly offset by a distance of 0.25 m from the 10 to the 20 s, which can be considered as the certain offset is acceptable in such highly dynamic. The height of the robot was always controlled at the desired value of 0.75 m, which indicated that the cascade control has a higher dynamic compensation accuracy based on the whole-body model, whereas LMPC and NMPC only controlled up to 0.73-0.735 m.

Both LMPC and NMPC are based on the single rigid body model. For a robot, the model accuracy is low for the robot with a leg to robot overall weight ratio of 31%. The height control accuracy, stability, and maximum forward velocity were not as high as MPC-THOC based on more accurate dynamics model with legs.

The maximum forward speed only reached 2.5 m/s in the walking gait because of the limitation of the stride frequency and leg length. Because of the increased clearance period, the speed of the robot can be higher under the running gait. This phenomenon will be studied in the future.

Case B) (Stable locomotion experiment under external interference)**:** To verify the controller stability in response to external interference, in this experiment, the impact forces were applied to the floating base for a certain time from the backward, lateral, and vertical downward directions during the locomotion process of the robot. After multiple tests, the maximum impulse that satisfies the dynamic balance is as follows: the impact force was 60 N along the positive direction of x-axis in the interval of 3.5-4 s, and the impulse is 30 N.s; the impact force of 115 N was applied along the positive direction of y-axis in the interval of 6.5-7 s, the impulse was 57.5 Ns; in the interval of 8.5-9 s, the impulse force was 150 N along the negative direction of z-axis, and the impulse was 75 Ns. Therefore, the corresponding Euler angle tracking curves of floating base are shown in Fig. 9, the velocity and height tracking curves are illustrated in Fig. 10.

In terms of attitude control performance: a) When receiving a backward impact in the 3.5-4 s interval, as the impulse accumulated, the first effect is that the pitch angle gradually increased in this interval and reached the maximum peak value -0.096 rad at the fourth second. Because the rotational moment formed by the impulse on the stand leg, the yaw angle was deflected considerably, with the positive and negative peak values reaching 0.173 rad and -0.16 rad, respectively, and the maximum peak value of roll angle was -0.145 rad. b) In the lateral impact in the 6.5-7-s interval, the most affected was the roll angle, which reached the maximum peak value of 0.17 rad at the

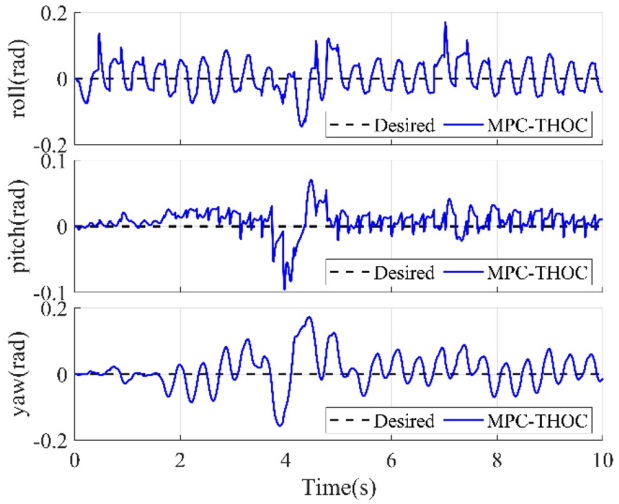

Fig. 9. Euler angle tracking curve of floating base.

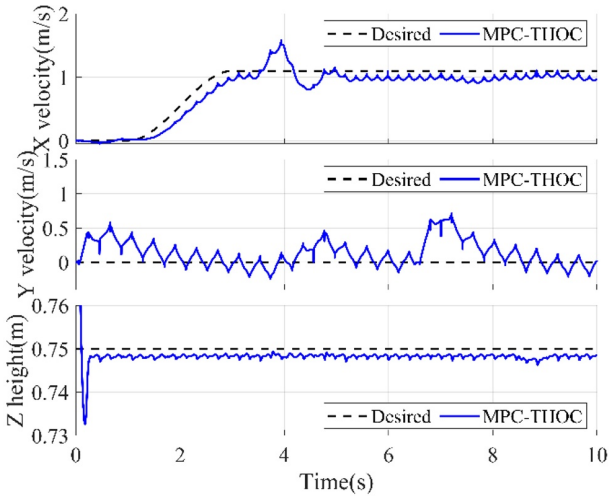

Fig. 10. The velocity and height tracking curves.

seventh second. Subsequently, the above-mentioned postures are quickly controlled within the steady-state fluctuation range of smaller amplitude through the action of cascade controller and the stand leg control that lasts for 1 s.

In terms of velocity and height control performance, in the backward impact, the forward velocity increased from 1 to 1.6 m/s. During the lateral impact, the lateral velocity increased from 0 to 0.7 m/s. When the robot deviated from desired velocity, the controller recalculated the foot location point and re-establishes a new balance point through multiple steps. The height decreased slightly after the impact, and then swiftly returned to the 0.75 m position.

Lateral and forward impulses render anti-interference challenging. Because the length of the sole was small, and the single sole was simplified into two points in the simulation, the friction force and torque formed on the ground were small, which limited the impulse range that the robot could bear. After exceeding the impulse amplitude studied in this study, the supporting leg slipped and the robot fell. Increasing the contact area between the sole and ground can be effectively increase anti-interference ability.

The cascaded control framework exhibits the antidisturbance performance of MPC and improves the stability of floating base posture and height control through task hierarchical optimization controller and considerably improves the forward velocity of walking gait dynamic motion of the robot to 2.5 m/s. In the simulation experiment, the physical 3D model of bipedal robot was used, which rendered the physical value to be close to the real object. Therefore, model prediction and task hierarchical optimization on the cascade antidisturbance control framework for robot dynamic locomotion can be used as a guideline for realizing dynamic control in physical objects.

7. CONCLUSION

THOC was combined with MPC under hierarchical optimization based on the whole-body model to accurately control the posture and height of floating base and better coordinate the stability of robot. Furthermore, the antidisturbance ability and locomotion velocity was improved. A novel cascade antidisturbance control framework that considered the dynamics of the legs was proposed to realize high dynamic locomotion of hydraulically driven bipedal robots. Two simulation experiments of high-velocity forward locomotion under walking gait and stable locomotion under external interference were performed. The antidisturbance performance of MPC was maintained. The maximum dynamic forward velocity increased considerably to 2.5 m/s, whereas that of NMPC was only 2.15 m/s.

In the future, the physical experiments of bipedal robot should be conducted to realize autonomous power and antidisturbance control. Furthermore, research on reinforcement learning and optimization methods is critical for achieving limited margin compensation and updating the dynamic model.

CONFLICT OF INTEREST

The authors declare that there is no competing financial interest or personal relationship that could have appeared to influence the work reported in this paper.

REFERENCES

[1] J. Pratt, C.-M. Chew, A. Torres, P. Dilworth, and G. Pratt, "Virtual model control; An intuitive approach for bipedal locomotion," *The International Journal of Robotics Research*, vol. 20, no. 2, pp. 129-143, 2001.

[2] S. Kajita, F. Kanehiro, K. Kaneko, K. Fujiwara, K. Harada, K. Yokou, and H. Hirukawa, "Resolved momentum con-

trol: humanoid motion planning based on the linear and angular momentum," *Proc. of IEEE/RSJ International Conference on Intelligent Robots & Systems*, IEEE, 2003.

[3] L. Sentis and O. Khatib, "Synthesis of whole-body behaviors through hierarchical control of behavioral primitives," *International Journal of Humanoid Robotics*, vol. 2, no. 4, pp. 505–518, 2005.

[4] S. Feng, E. Whitman, X. Xinjilefu, and C. G. Atkeson, "Optimization based full body control for the DARPA robotics challenge," *Journal of Field Robotics*, vol. 2, pp. 143-156, 2015.

[5] S. G. Mcgiil, S.-J. Yi, H. Yi, M. S. Ahn, S. Cho, K. Liu, D. Sun, B. Lee, H. Jeong, J. Huh, D. Hong, and D. D. Lee, "Team THOR's entry in the DARPA robotics challenge finals 2015," *Journal of Field Robotics*, vol. 34, no. 4, pp. 775-801, 2018.

[6] M. Johnson, B. Shrewsbury, S. Bertrand, T. Wu, D. Duran, M. Floyd, P. Abeles, D. Stephen, N. Mertins, A. Lesman, J. Carff, W. Rifenburgh, P. Kaveti, W. Straatman, J. Smith, M. Griffoen, B. Layton, T. de Boer, T. Koolen, P. neuhauss, and J. Pratt, "Team IHMC's lessons learned from the DARPA robotics challenge trials," *Journal of Field Robotics*, vol. 32, no. 2, pp. 192-208, 2015.

[7] D. KIm, Y. Zhao, G. Thomas, B. R. Fernandez, and L. Sentis, "Stabilizing series-elastic point-foot bipeds using whole-body operational space control," *IEEE Transactions on Robotics*, vol. 32, no. 6, pp. 1362- 1379, 2016.

[8] D. Kim, S. J. Jorgensen, J. Lee, J. Ahn, J. Luo, and L. Sentis, "Dynamic locomotion for passive-ankle biped robots and humanoids using whole-body locomotion control," *The International Journal of Robotics Research*, vol. 39, no. 8, pp. 936-956, 2020.

[9] F. L. Moro, M. Gienger, A. Groswami, N. G. Tsagarakis, and D. G. Caldwell, "An attractor-based whole-body motion control (WBMC) system for humanoid robots," *Proc. of 13th IEEE-RAS International Conference on Humanoid Robots (Humanoids)*, IEEE, 2015.

[10] S. Kuindersma, F. N. Permentera and R. Tedrake, "An efficiently solvable quadratic program for stabilizing dynamic locomotion," *Proc. of IEEE International Conference on Robotics and Automation (ICRA)*, IEEE, 2014.

[11] P. M. Wensing and D. E. Orin, "Improved computation of the humanoid centroidal dynamics and application for whole-body control," *International Journal of Humanoid Robotics*, vol. 13, no. 1, 1550039, 2016.

[12] G. Raiola, E. M. Hoffman, M. Focchi, N. Tsagarakis, and C. Semini, "A simple yet effective whole-body locomotion framework for wuadruped robots," *Frontiers in Robotics and AI*, vol. 7, 2020.

[13] F. Farshidian, E. Jelavi, A. W. Winkler, and J. Buchli, "Robust whole-body motion control of legged robots," *Proc. of IEEE/RSJ International Conference on Intelligent Robots and Systems (IROS)*, IEEE, 2017.

[14] S. Fahmi, C. Mastalli, M. Focchi, and C. Semini, "Passive whole-body control for quadruped robots: Experimental validation over challenging terrain," arxiv: Robotics, 2018.

[15] C. D. Bellicoso, F. Jenelten, P. Fankhauser, C. Gehring, J. Hwangbo, and M. Hutter, "Dynamic locomotion and whole-body control for quadrupedal robots," *Proc. of IEEE/RSJ International Conference on Intelligent Robots & Systems (IROS)*, IEEE, 2017.

[16] E. Jelavic and M. Hutter, "Whole-body motion planning for walking excavators," *Proc. of IEEE/RSJ International Conference on Intelligent Robots and Systems (IROS)*, IEEE, 2019.

[17] K. Yuan and Z. Li, "An improved formulation for model predictive control of legged robots for gait planning and feedback control," *Proc. of IEEE/RSJ International Conference on Intelligent Robots and Systems (IROS)*, IEEE, 2018.

[18] J. A. Castano, Z. Li, C. Zhou, N. Tsagarakis, and D. Caldwell, "Dynamic and reactive walking for humanoid robots based on foot placement control," *International Journal of Humanoid Robotics*, vol. 13, no. 2, 1550041, 2016.

[19] D. Yoon, B. Kim, I. Jo, and W. Jeong, "A dynamic locomotion strategy for stair walking of a quadruped robot," *Proc. of 18th International Conference on Ubiquitous Robots (UR)*, 2021.

[20] G. Bledt and S. Kim, "Implementing regularized predictive control for simultaneous real-time footstep and ground reaction force optimization," *Proc. of IEEE/RSJ International Conference on Intelligent Robots and Systems (IROS)*, IEEE, 2019.

[21] L. Ishihara, T. D. Itoh, and J. Morimoto, "Full-body optimal control toward versatile and agile behaviors in a humanoid robot," *IEEE Robotics and Automation Letters*, vol. 5, no. 1, pp. 119-126, 2020.

[22] A. Mukovskiy, C. Vassallo, M. Naveau, O. Stasse, P. Souères, and M. A. Giese, "Adaptive synthesis of dynamically feasible full-body movements for the humanoid robot HRP-2 by flexible combination of learned dynamic movement primitives," *Robotics & Autonomous Systems*, vol. 91, pp.270-283, 2017.

[23] D. Limon, I. Alvarado, T. Alamo, and E. F. Camacho, "Robust tube-based MPC for tracking of constrained linear systems with additive disturbances," *Journal of Process Control*, vol. 20, no. 3, pp. 248-260, 2010.

[24] M. Zhao, C.-C. Jiang, and M.-H. She, "Robust contractive economic MPC for nonlinear systems with additive disturbance," *International Journal of Control, Automation, and Systems*, vol. 16, no. 5, pp. 2253-2263, 2018.

[25] P. Bumroongsri, "Tube-based robust MPC for linear time-varying systems with bounded disturbances," *International Journal of Control, Automation, and Systems*, vol. 13, no. 3, pp. 620-625, 2015.

[26] T. Zhang, G. Kahn, S. Levine, and P. Abbeel, "Learning deep control policies for autonomous aerial vehicles with MPC-guided policy search," *Proc. of IEEE International Conference on Robotics and Automation (ICRA)*, 2016.

[27] L. B. Hamouda, M. Ayadi, and N. Langlois. "Fuzzy fault tolerant predictive control for a diesel engine air path," *International Journal of Control, Automation, and Systems*, vol. 14, no. 2, pp. 443-451, 2016.

[28] J. di Carlo and P. M. Wensing. "Dynamic locomotion in the MIT Cheetah 3 through convex model-predictive control," *Proc. of IEEE/RSJ International Conference on Intelligent Robots and Systems (IROS)*, 2018.

[29] R. Grandia and F. Farshidian. "Feedback MPC for torque-controlled legged robots," *Proc. of IEEE/RSJ International Conference on Intelligent Robots and Systems (IROS)*, 2019.

Jie Huang received his B.S. and M.S. degrees in mechanical and electrical engineering from Central South University, in 2008 and 2011, respectively, and engaged in technology research and development in Zoomlion Heavy Industry Science and Technology Co., Ltd. from 2011 to 2017, then received a Ph.D. degree from National University of Defense Technology (NUDT) in 2021. His research interests include legged robot trajectory optimization, high-performance motion control, and formation control.

Huajie Hong received his Ph.D. degree from National University of Defense Technology. His research interests include key technologies such as optimal design and manufacturing of electromechanical servomechanics, embeded electromechanical control systems, optical-electromechanical integration mechanisms and control, and optical image tracking control theory and algorithm.

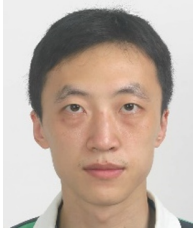

Nan Wang received his B.S. degree in automatic control from the College of Mechatronics and Automation, National University of Defense Technology (NUDT), Changsha, China, in 2003, and his M.S. and Ph.D. degrees in control science and engineering from the College of Mechatronics and Automation, NUDT, in 2005 and 2012, respectively, where he is currently an Associate Professor with the College of Intelligence Science and Technology. He has published more than ten articles in international journals and conferences and has coauthored one book. His research interests include mission planning, autonomous control, and collaboration of unmanned systems. He has served as an Academic Editor for the Tactical Missile Technology.

Hongxu Ma received his B.S. degree in automatic control in 1988, an M.S. degree in intelligent control in 1991, a Ph.D. degree in control science and control engineering from National University of Defense Technology in 1995. In 1995, he stayed in the school for research work. He is currently a professor at the National University of Defense Technology. He is mainly engaged in the research of foot robots. In 2000, he realized the dynamic walking of Chinese two-legged robots for the first time. He has published more than 150 high-level academic papers, published 1 monograph, and authorized more than 10 patents.

Honglei An received his B.S., M.S., and Ph.D. degrees from National University of Defense Technology, in 2006, 2009, and 2013, respectively. From 2013 to 2019, he is a lecturer in NUDT. His research interests include legged robot control, nonlinear control theory, and optimal control application.

Lin Lang received his B.S., M.S., and Ph.D. degrees from National University of Defense Technology, in 2006, 2009, and 2016, respectively. From 2018, he is a lecturer in Hunan University of Finance and Economics. His research interests include legged robot control and nonlinear control theory.